The Astrophysical Journal Letters, 769:L33 (7pp), 2013 June 1 doi:10.1088/2041-8205/769/2/L33

OBSERVATION OF MAGNETIC RECONNECTION DRIVEN BY GRANULAR SCALE ADVECTION

Zhicheng Zeng[1,2], Wenda Cao[1,2], and Haisheng Ji[2,3]
[1] Center for Solar-Terrestrial Research, New Jersey Institute of Technology, 323 Martin Luther King Blvd., Newark, NJ 07102, USA
[2] Big Bear Solar Observatory, 40386 North Shore Lane, Big Bear City, CA 92314, USA
[3] Purple Mountain Observatory, CAS, Nanjing 210008, China
Received 2013 February 26; accepted 2013 May 2; published 2013 May 16

ABSTRACT

We report the first evidence of magnetic reconnection driven by advection in a rapidly developing large granule using high spatial resolution observations of a small surge event (base size $\sim 4'' \times 4''$) with the 1.6 m aperture New Solar Telescope at the Big Bear Solar Observatory. The observations were carried out in narrowband (0.5 Å) He I 10830 Å and broadband (10 Å) TiO 7057 Å. Since He I 10830 Å triplet has a very high excitation level and is optically thin, its filtergrams enable us to investigate the surge from the photosphere through the chromosphere into the lower corona. Simultaneous space data from the Atmospheric Imaging Assembly and Helioseismic and Magnetic Imager on board the *Solar Dynamics Observatory* were used in the analysis. It is shown that the surge is spatio-temporally associated with magnetic flux emergence in the rapidly developing large granule. During the development of the granule, its advecting flow ($\sim$2 km s^{-1}) squeezed the magnetic flux into an intergranular lane area, where a magnetic flux concentration was formed and the neighboring flux with opposite magnetic polarity was canceled. During the cancellation, the surge was produced as absorption in He I 10830 Å filtergrams while simultaneous EUV brightening occurred at its base. The observations clearly indicate evidence of a finest-scale reconnection process driven by the granule's motion.

Key words: Sun: activity – Sun: chromosphere – Sun: photosphere

Online-only material: animation, color figures

1. INTRODUCTION

The solar chromosphere has been known to be very dynamic and is a sea of small-scale activity such as microflares, Ellerman bombs, and surges (Fang et al. 2006). Recent observations made by *Hinode* and large ground-based solar telescopes have discovered that the chromosphere is even more dynamic than previously thought (Shibata et al. 2007; Nishizuka et al. 2008; Goode et al. 2010b). It is believed that such activity is actually activated and driven by photospheric dynamics which exhibits a constantly evolving, multipolar magnetic flux distribution. However, how convective motion and flows in the photosphere activate and drive solar activity is still an open question. Using observations to answer this kind of question has proven to be challenging. With the advent of large ground-based solar telescopes with adaptive optics (AO) and state-of-the-art instruments, observing and studying small-scale activity will provide us less ambiguous information about the physical mechanism, since major events contain many couplings of smaller spatial scale energy release processes.

Surges, which can be precisely pinned down to the photosphere with their small spatial scales, are the most suitable observational targets to reveal the physical links between activities in the photosphere and upper atmosphere. A surge is the phenomenon of straight or slightly curved mass ejections shooting out from a brightened chromosphere patch up to coronal heights with speeds of 20–200 km s^{-1} (Rust 1968) and lifetimes of 10–20 minutes (Sterling 2000). Hα surges can be visible in EUV/UV and even soft X-ray, i.e., cool and hot ejected components coexist in the same ejection event (Rust et al. 1977; Schmahl 1981). Historically, the term "surge" and "jet" refer to the cool and hot ejected plasma, respectively. Surges show a strong trend for recurrence, being associated with magnetic flux emergence and cancellation around their bases in the photosphere (Kurokawa & Kawai 1993; Liu & Kurokawa 2004). Previous observations support the idea that magnetic reconnection between emerging flux and overlying magnetic field plays a key role in powering a surge model (Shibata et al. 1992; Canfield et al. 1996; Shimojo et al. 1998; Chae et al. 1999).

Hα and Ca II 8542 Å spectral lines are mostly used to probe the chromospheric activity. However, due to their opaque nature, it is not easy to obtain exactly cospatial photospheric information simultaneously. He I 10830 Å imaging has a predominant advantage in this aspect and has proven to be a unique choice for high-resolution observations (Vrsnak et al. 2002; Ji et al. 2012). The line has a high excitation level reflecting the solar upper chromosphere, and the most important feature is that the line is optically thin, thus allowing the photosphere to be shining through. The granulation in the background of 10830 Å filtergrams gives us irreplaceable aid for pinning exactly down the small-scale activity in the photosphere.

Observing small-scale activity with 10830 Å triplet is a timely topic with the advent of the 1.6 m aperture New Solar Telescope at the Big Bear Solar Observatory (NST/BBSO; Goode et al. 2010a; Cao et al. 2010b). Its off-axis design can vastly reduce stray light since there is no central obscuration. The site's good seeing conditions combined with the high-order AO system enable observations with a spatial resolution close to the diffraction limit.

2. OBSERVATION AND DATA REDUCTION

The observations were carried out on 2011 July 22, targeting coronal loops in solar active region NOAA 11259, with narrow band (bandpass: 0.5 Å) in He I 10830 Å, narrow band (bandpass: 0.25 Å) in Hα 6563 Å in the blue wing (-0.65 Å), and broad band (bandpass: 10 Å) of TiO 7057 Å lines. The 10830 Å narrowband filter was tuned to -0.25 Å, making the filtergram more sensitive to upward moving features. With the aid of

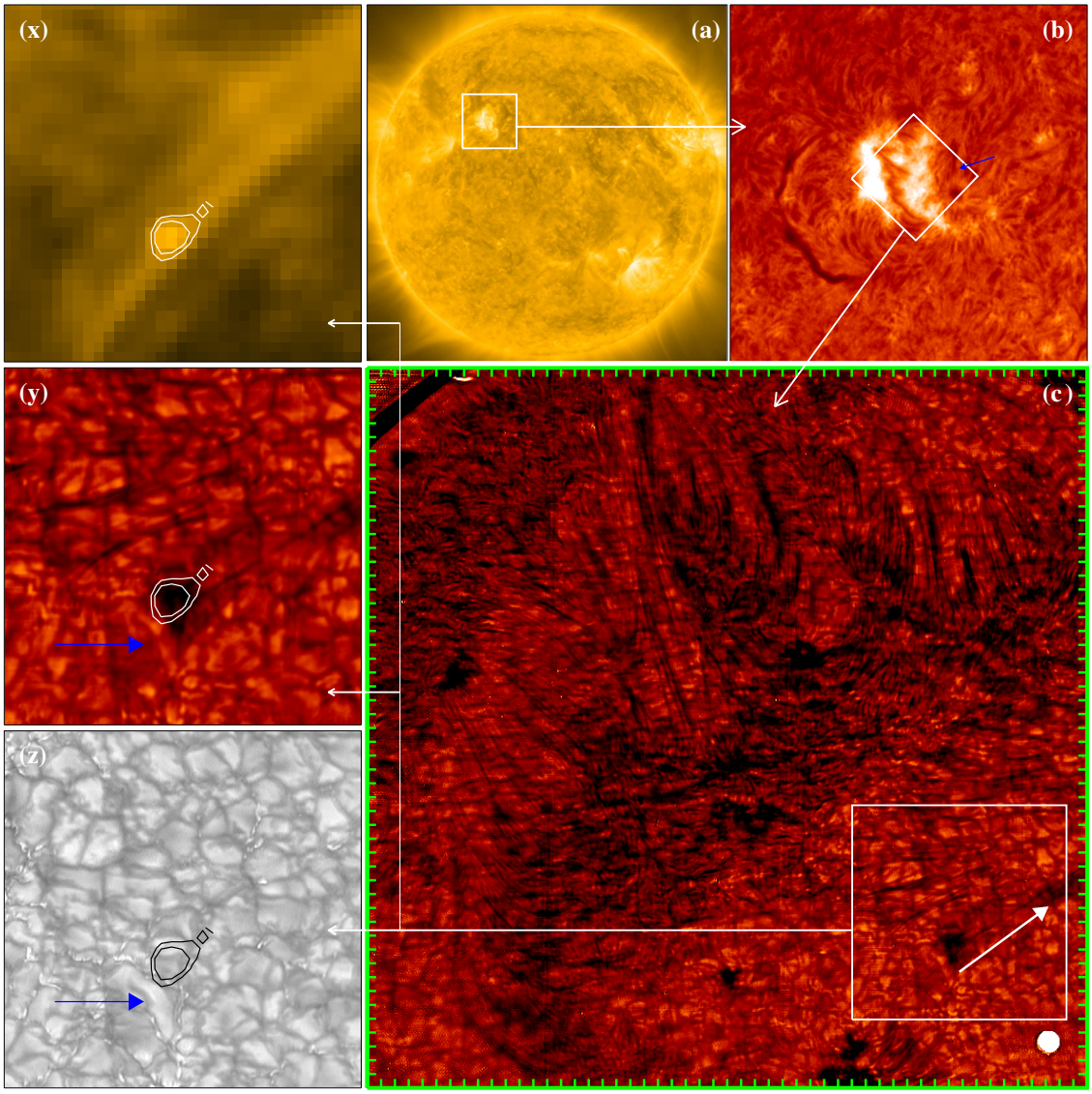

Figure 1. (a) Full-disk image of the Sun observed at 171 Å by AIA/*SDO*. The white box depicts the active region NOAA 11259. (b) A subregion of BBSO full-disk Hα filtergram at 17:48:03 UT. The blue arrow points to the surge. (c) A sample 10830 Å filtergram at 17:45:35 UT observed with the NST/BBSO. The surge appears as an elongated dark feature along the direction indicated by the white arrow. The boxed area in panel (c) is enlarged and shown in three different wavelengths on panels (x)–(z) with contours representing the 171 Å emission. (x) 171 Å emission (17:45:36 UT). (y) 10830 Å filtergram. (z) TiO image (17:45:40 UT). The blue arrows in panels (x) and (y) point to the large granule associated with the surge. Each box in the panels depicts the field of view of the subsequent frames(s) indicated by corresponding white arrow(s).

(An animation and a color version of this figure are available in the online journal.)

high-order AO (Cao et al. 2010b) and speckle reconstruction post-processing (KISIP speckle reconstruction code; Wöger & von der Lühe 2007), diffraction-limited resolution images at the three bands were achieved. The cadences at TiO, Hα, and He I were all 15 s. A high sensitivity HgCdTe CMOS infrared focal plane array camera (Cao et al. 2010a) was employed to acquire the 10830 Å data. TiO molecular bands are sensitive to temperature, thus enhancing the contrast of intensity in the photosphere, due to the stronger absorption of these bands in dark cool intergranular lanes.

For investigating the million degree coronal plasma and the evolution of magnetic field, simultaneous data from the *Solar Dynamics Observatory* (*SDO*; Lemen et al. 2012) were downloaded. In this Letter, the *SDO* data include EUV data from the Atmospheric Imaging Assembly (AIA), full-disk continuum images, and line-of-sight magnetogram from the Helioseismic and Magnetic Imager (HMI; Schou et al. 2012). Spatial co-alignment among these data was done by co-aligning the HMI continuum images with the NST TiO data, and then co-aligning the TiO data with the 10830 Å filtergrams. We used sunspots and especially groups of bright granules for co-alignment. Owing to a multiplicity of common features (bright granulation), it was straightforward to precisely align the HMI/*SDO* continuum images with the NST He I and TiO images. The accuracy of the co-alignment is better than 0.″5. Since *SDO* images are already co-aligned before being available for downloading, HMI continuum images can serve as the intermediary for co-alignment between the AIA images and the NST images.

3. RESULTS

An overview of the surge event is shown in Figure 1. The surge spurted out in the vicinity of the leading sunspot in the

active region NOAA 11259, lasting from 17:33 to 17:55 UT. A full-disk AIA 171 Å image (Figure 1(a)) shows the location and corona loop system of the targeted active region, which is encompassed by a white box. Each box in the panels depicts the field of view of subsequent frame(s) indicated by white arrow(s). Figure 1(b) is a subregion of a full-disk Hα filtergram observed with the BBSO 10 cm aperture telescope. Two ribbon-like plage regions are the footpoint regions of the EUV loop system. In low-resolution Hα images, the surge is faint and ephemeral. It only appears at 17:48:03 UT as a faint dark feature, indicated by a blue arrow in panel (b). A snapshot of the NST He I 10830 Å filtergram with a field of view of 52×52 Mm is given in Figure 1(c), which clearly shows the ultrafine loop structure. The loops connect two heavily absorbed regions, which correspond to Hα plages. A striking feature is that the cross section of the loops remains almost constant ($\sim$100 km) over long distances (Ji et al. 2012). Also, photospheric background is shining through in the 10830 Å filtergrams and we can roughly see the granules and intergranular lanes.

The surge appeared as a darkened area erupting along the direction denoted by the white arrow. The surge is of small scale, with a base size of $\sim 4'' \times 4''$. The spine of the surge looks threaded and the thickness of each thread is about $0''.1$. The apparent width and maximum length of the threaded spine are 1–2 Mm and 18–20 Mm, respectively. The ejecta travel along surge's threaded spine with maximum apparent velocity about 42 km s^{-1} and finally fade away. The boxed area in panel (c) is enlarged, shown in the left three panels (x)–(z). Panel (x) shows simultaneous EUV 171 Å brightening. The brightening's contours are overlaid on the enlarged 10830 Å filtergram (panel (y)) and a corresponding TiO image (panel (z)). An apparent corona loop, which is running across the surge, was seen to slightly light up during the surge. Strong EUV emission and 10830 Å absorption are cospatial at the base of the surge as shown in Figure 1(y). Taking advantage of six filter wavelength EUV data from AIA/*SDO*, we use a method developed by Aschwanden et al. (2013) to calculate the emission measure at the footpoint of the surge during the second peak of the surge eruption. Then, according to the relation $Eth = 3kT\sqrt{EM \cdot V}$, the estimated thermal energy is about 4.3×10^{26} erg. A large developing granule (indicated by a blue arrow in panels (y) and (z)) expands and squeezes the material toward the intergranular lane area where the surge spurted out. A series of bright points were formed during the squeezing. An online animation (NST_surge.mpg) made of the 10830 Å filtergrams is available, with simultaneous TiO images overlaid with the surge (pink) extracted from the filtergrams.

As reported by Shimojo et al. (1998), most of the jets are produced in satellite polarity (polarity opposite to nearby sunspot) type region. The surge in this Letter also was associated with the emergence of satellite polarity magnetic flux. We co-aligned the images at TiO and 10830 Å, as well as a simultaneous HMI line-of-sight magnetogram, and created the composite image shown in Figure 2. The gray background is the TiO image and the pink features, which are distributed cospatially with the intergranular lanes, stand for the absorbing features extracted from 10830 Å filtergram. The red and blue contours represent the positive and negative magnetic field, respectively. In this figure, the excellent co-alignment of HMI magnetogram and NST photospheric image can be clearly seen from the correspondence between magnetic concentration and bright points. The root of the surge (the pink feature inside the dotted box) is just sitting on the intergranular lane area beside the aforementioned large granule. Positive magnetic flux concentration is formed in the intergranular lane area and pushed into the nearby negative magnetic field area due to the advecting motion of the developing granule. The strongest magnetic field strength is about 300 G. Considering filling factor, the field there may reach or exceed 1000 G.

By further looking into the time sequence images, we find clearer evidence of the surge's association with granular motion, magnetic field concentration, and cancellation. In Figure 3, the evolution of the surge is shown in two 10830 Å filtergrams (a1 and b1). The underlying developing granule can be clearly seen and the surge anchors to the intergranular lane area throughout. To make the scenario clearer, the absorption features (pink) from Figure 3(a1) to (b1) are extracted and overlaid on simultaneous TiO images ((a2) and (b2)). The black circles indicate the location of the surge footpoint. The Fourier local correlation tracking method (FLCT; Fisher & Welsch 2008) was applied to the time sequence to derive horizontal proper motions. In Figure 3(a2), the flow maps are presented with the length and direction of the arrows indicating the average velocity vector. The developing granule is squeezing the lane area at the surge footpoint with outstanding advection speed of 2 km s^{-1} at its front, which is higher than the typical speed of granules ($\sim$0.5 km s^{-1}).

In Figures 3(1)–(5), a time series of contours of line-of-sight magnetic field are shown. Red and blue contours represent positive and negative magnetic fields, respectively. Simultaneous TiO images are presented in Figures 3(3)–(5) when they are available. According to the change of the contours' morphology, there is an obvious increment in both positive magnetic flux beside the surge base and a "U"-shaped negative magnetic flux below, indicating emergence of a bipole. The positive magnetic flux emerged as shown by the increasing area of red contour near the center from Figure 3(1)–(3). In Figure 3(4), the area of the strongest red contour decreased comparing with previous panels, indicating the ongoing magnetic cancellation. The large granule pushed the emerged positive flux toward the intergranular lane area, as shown by the upward shifting of the red contours on the granule.

The granular flow advected the magnetic flux and, meanwhile, the positive magnetic concentration seems to suppress the development of the granule. The picture is consistent with the findings made by Zhang et al. (2009) using *Hinode* data. Also, in Figures 3(4) and 3(5), the blue contour for the negative magnetic field near the surge footpoint decays obviously, indicating the cancellation of the negative field. The phenomenon suggests that the pre-existing field is canceled by the newly emerging opposite polarity flux during the surge.

Figure 4 shows the time profiles of the surge. Panel (a) is the light curve of the surge footpoint in 10830 Å, while panels (b) and (c) represent positive and negative magnetic fluxes, respectively. These magnetic fluxes are calculated within the boxed area in Figure 2. Panel (d) gives three samples of EUV emission time profile at 171 Å (dotted line), 94 Å (solid line), and 131 Å (dash line) as observed by AIA/*SDO*. The curves in panels (a) and (d) are both normalized with respect to their own maximum values. There are three depressions in the 10830 Å time profile (separated by vertical dash lines), representing three main stages in the surge process. Before the surge, there is a steep increment of the positive flux starting at 17:31 UT. Then two minutes later, the surge spurts out immediately after the obvious cancellation of the negative flux. The negative flux varies significantly, although the signal is much weaker than the

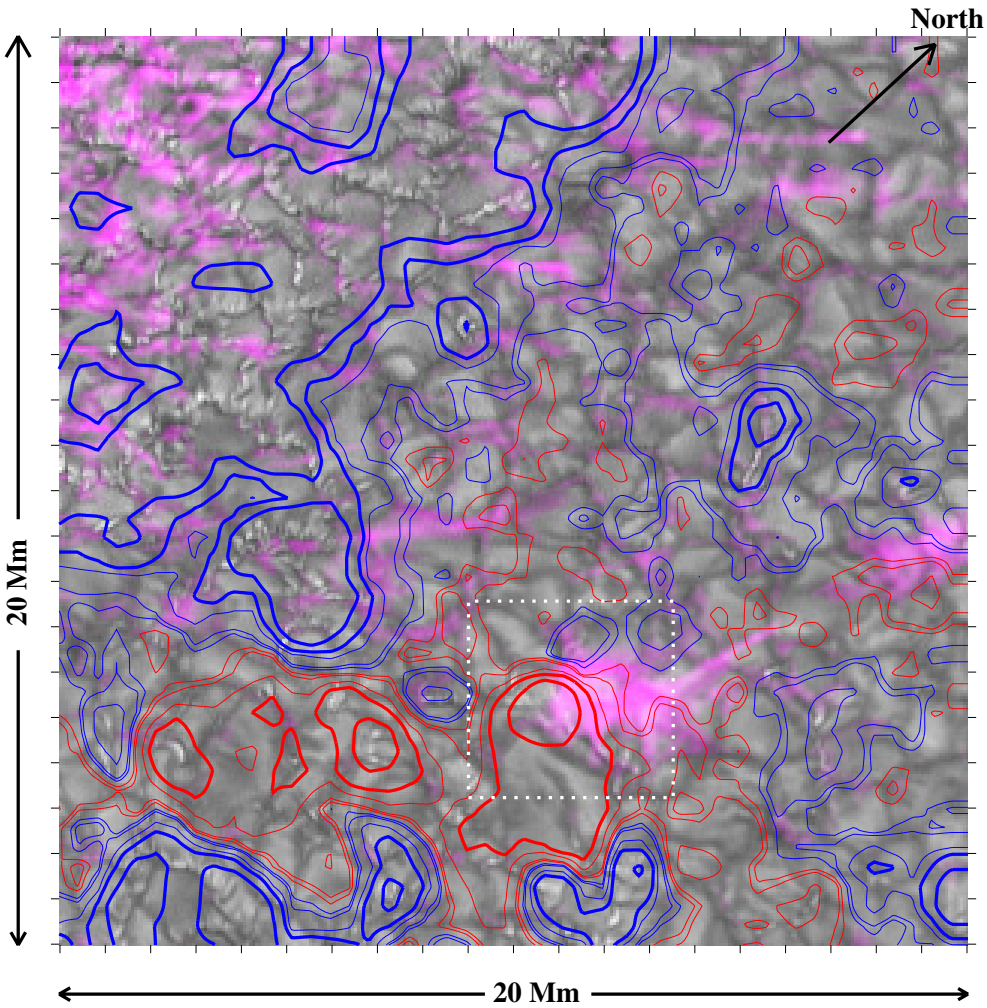

Figure 2. Composite image overlaid with line-of-sight magnetogram (17:42:45 UT) obtained by HMI/*SDO*. The composite image is made of a TiO image (gray, 17:42:25 UT) and absorbing features (pink) extracted from a 10830 Å filtergram (17:42:22 UT). Red and blue contours represent positive and negative magnetic field, respectively. The contour levels are ±5, ±10, ±30, ±50 (thick contours), and ±100 G (thick contours), respectively. The white dotted box depicts the area for magnetic flux calculation in Figure 4.

(A color version of this figure is available in the online journal.)

positive flux. After the positive magnetic flux stops increasing around 17:40 UT, it decreases slightly during the violent second stage of the surge. Basically, all three stages in the 10830 Å time profile have corresponding bumps in each of the EUV curves. However, there are some differences for the EUV responses. During the first stage, the EUV 171 Å signal can hardly be seen and the emissions of 94 Å and 131 Å are barely above noise level compared with the subsequent obvious enhancement in the second stage. The 171 Å spectrum line has a characteristic temperature of ∼0.7 MK (log $T \sim 5.85$), while both 94 Å (log $T \sim 6.8$) and 131 Å (log $T \sim 7$) have higher characteristic temperatures of ∼7 MK, which implies that the corresponding temperature of the surge is much higher in the beginning even though EUV emissions are weaker.

4. DISCUSSIONS AND CONCLUSIONS

With the NST's high spatial resolution imaging observations as well as simultaneous space data from AIA and HMI on board *SDO*, we give a detailed analysis of a small surge event and find the first evidence of magnetic reconnection driven by advection in a rapidly developing large granule. Such a small event would have been neglected in low-resolution observations; however, it proves to be valuable for exploring the physical mechanism of small-scale activity. Furthermore, granulation in the background of He I 10830 Å filtergrams offers great help in precisely pinning the granular scale surge down to the photosphere. High-resolution Hα data are not shown in this Letter since they give no new results.

We present a very clear picture that there is an emergence of a magnetic bipole associated with the surge, while the positive emerging flux is accompanied by the development of a large granule. The granule's advection pushed the positive magnetic flux into an intergranular lane area, causing magnetic concentration there and canceling nearby negative flux. The negative magnetic flux canceled during the surge is about 6.2×10^{17} Mx. Assuming that reconnection happens in a cubic box ∼2.1 Mm^3, within which the magnetic field is uniformly distributed, the released magnetic energy could be estimated to be 1.2×10^{26} erg, which is comparable to the thermal energy estimated in previous section. This supports the picture that the surge is a result of the magnetic reconnection directly driven by the granule's advection.

Our observations are consistent with the observations made by Shimojo et al. (1998). The surge resulted from the emergence of satellite polarity. As a matter of fact, the total positive

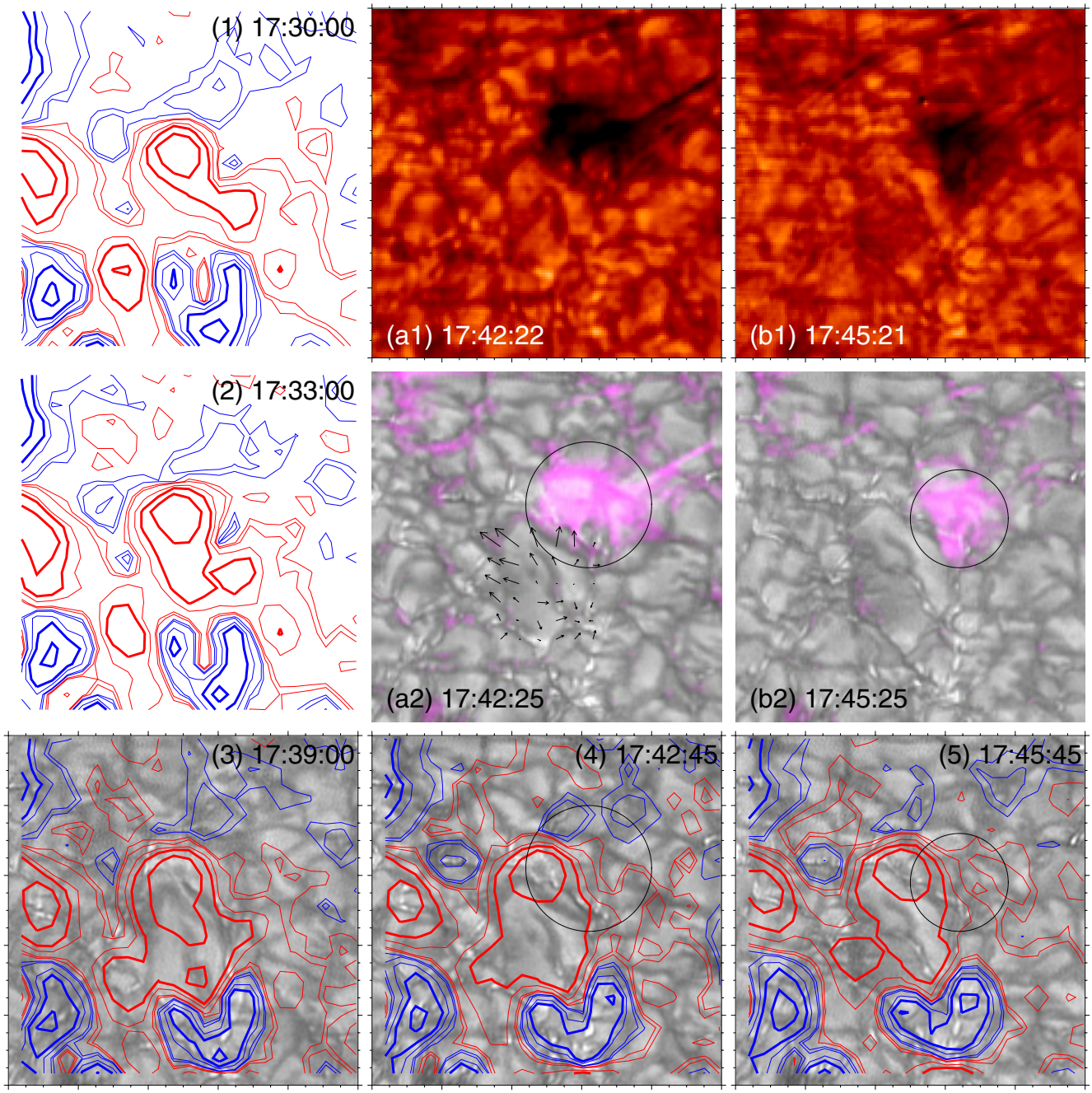

Figure 3. ((a1) and (b1)) He I 10830 Å filtergrams showing the evolution of the surge and underlying granules. ((a2) and (b2)) Simultaneous TiO images (gray) overlaid with the surge (pink) extracted from panels (a1) and (b1). The black circles encompass the surge's roots, which anchor in the intergranular area. In panel (a2), we plot the transverse proper motion obtained through FLCT method on the large granule beside the surge, with maximum speed about 2 km s^{-1}. (1)–(5) Time series of contours of line-of-sight magnetic field. The contours are overlaid on simultaneous TiO images when they are available. Red and blue contours represent positive and negative magnetic fields, respectively, with contour levels at ±10, ±30, ±50 (thick contours), and ±100 G (thick contours). The field of view of these images is 10 × 10 Mm.

(A color version of this figure is available in the online journal.)

magnetic flux was increasing because the positive magnetic field was dramatically emerging. However, when the emergence reached its peak, the positive magnetic flux decrement became visible, which was caused by cancellation with the opposite negative magnetic flux. This corresponds to the second eruption of the surge.

Chae et al. (1999) proposed a two-step reconnection model based on the fact that they found magnetic cancellation before the EUV brightening. For the surge event in this Letter, this two-step assumption could be supported if there were no 10830 Å and 94 Å observations. However, both excitation of helium and brightening of 94 Å could be seen as soon as the negative magnetic flux was canceled, which means the magnetic cancellation and reconnection occurred simultaneously.

In order to have 10830 Å absorption, electrons must be excited to the lowest triplet state of helium atoms. Three distinct mechanisms have been proposed, namely, photoionization–recombination mechanism (PRM), collisional mechanism

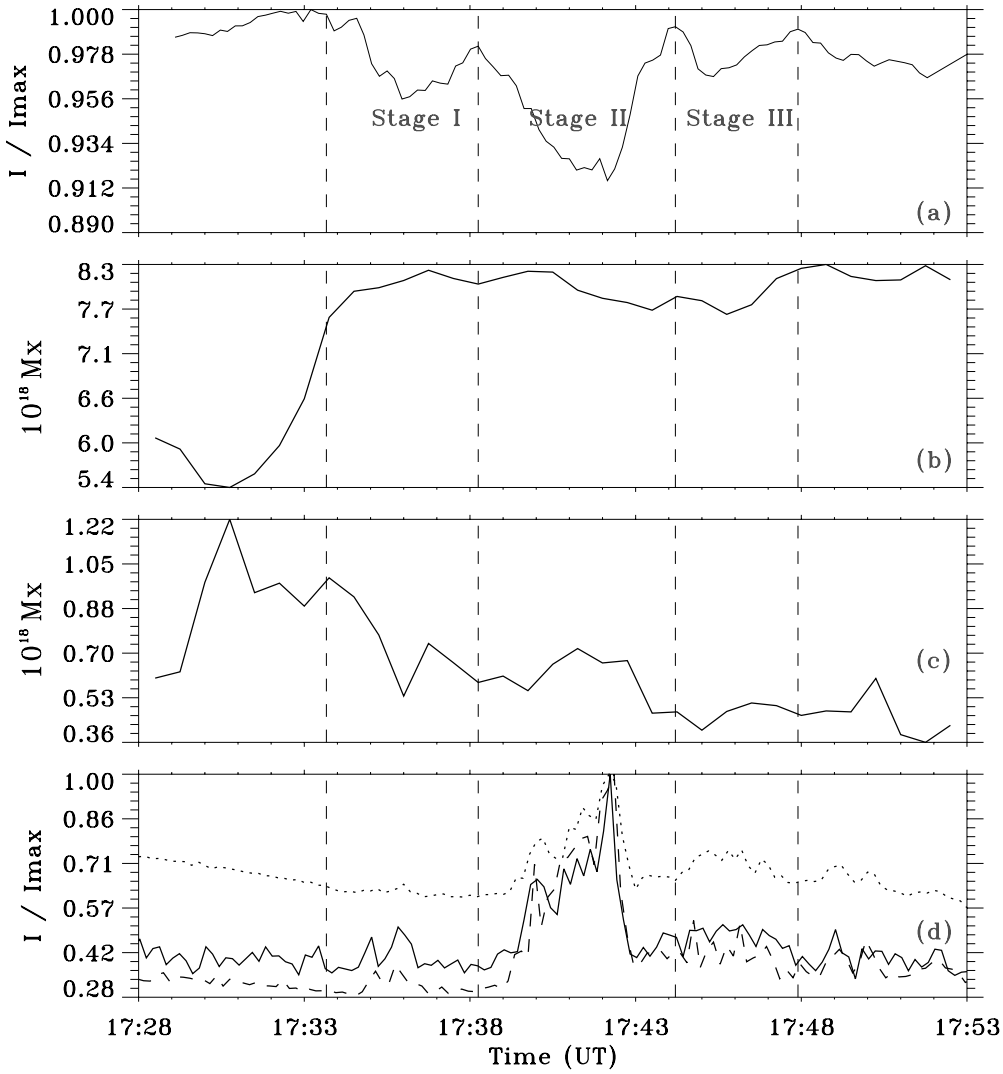

Figure 4. (a) Light curve at the surge's base in He I 10830 Å observation. According to the darkening at its base, the surge is separated into three main stages using the vertical dashed line. Panels (b) and (c) give the positive and negative magnetic flux time profiles in the boxed area in Figure 2, respectively. (d) Counterpart of EUV emission profiles at 171 Å (dotted line), 94 Å (solid line), and 131 Å (dash line) as observed by AIA/*SDO*. The curves in panels (a) and (d) are normalized with respect to their own maximum values.

(CM), and collisional ionization followed by recombination mechanism (CRM; Ding et al. 2005). For the surge analyzed here, the formation of 10830 Å absorption is complicated. As shown in Figure 4, during the second depression, where variations of 10830 Å absorption and EUV emissions are cotemporal, we favor the PRM as the primary mechanism of the 10830 Å absorption. However, for the first depression, there are no apparent EUV signals in most AIA channels except weak emissions from 94 Å and 131 Å. Compared to the third stage, which has stronger EUV emission but weaker 10830 Å absorption, we do not believe there are enough EUV photons to raise the strong He I 10830 Å absorption in the first stage. Thus, CM and CRM should be taken into account. Furthermore, considering AIA's EUV response functions, the temperature during the first depression can be deduced as high as ~7 MK. These superhot electrons may play an important role in producing stronger He I absorption during the first stage.

This granule advection triggering surge implies that magnetic reconnection occurrs on quite small spatial scales throughout the solar atmosphere and these ubiquitous small-scale reconnections may play an important role in heating the upper atmosphere. However, it is not clear whether granular advection is indispensable in all small-scale activity in the upper atmosphere. A more detailed statistics is needed and will be presented in a subsequent paper. With the high-resolution observations, the examination of interrelation between photospheric motions and overlying small-scale activity no doubt will shed new light on uncovering the nature of small-scale activity in the dynamic chromosphere.

We thank the BBSO observing staff and instrument team for their support. *SDO* is a project of NASA. Z.Z. and W.C. acknowledge the support of the U.S. NSF (AGS-0847126 and AGS-1146896), NASA (NNX08BA22G), and AFOSR (FA 2386-12-1-3018 and FA9550-09-1-0655). H.J. acknowledges the support by NSFC grants, 11173062, 10833007, 10921303, 11178002, and the 973 program under grant 2011CB811402.

REFERENCES

Aschwanden, M. J., Boerner, P., Schrijver, C. J., & Malanushenko, A. 2013, SoPh, 283, 5
Canfield, R. C., Peardon, K. P., Leka, K. D., et al. 1996, ApJ, 464, 1016

Cao, W., Coulter, R., Gorceix, N., & Goode, P. R. 2010a, Proc. SPIE, 7742, 774220
Cao, W., Gorceix, N., Coulter, R., et al. 2010b, AN, 331, 636
Chae, J., Qiu, J., Wang, H., & Goode, P. R. 1999, ApJL, 513, L75
Ding, M. D., Li, H., & Fang, C. 2005, A&A, 432, 699
Fang, C., Tang, Y. H., Xu, Z., Ding, M. D., & Chen, P. F. 2006, ApJ, 643, 1325
Fisher, G. H., & Welsch, B. T. 2008, in ASP Conf. Ser. 383, Subsurface and Atmospheric Influences on Solar Activity, ed. R. Howe, R. W. Komm, K. S. Balasubramaniam, & G. J. D. Petrie (San Francisco, CA: ASP), 373
Goode, P. R., Coulter, R., Gorceix, N., Yurchyshyn, V., & Cao, W. 2010a, AN, 331, 620
Goode, P. R., Yurchyshyn, V., Cao, W., et al. 2010b, ApJL, 714, L31
Ji, H., Cao, W., & Goode, P. R. 2012, ApJL, 752, L25
Kurokawa, H., & Kawai, G. 1993, in ASP Conf. Ser. 46, IAU Colloq. 141: The Magnetic and Velocity Fields of Solar Active Regions, ed. H. Zirin, G. Ai, & H. Wang (San Francisco, CA: ASP), 507
Lemen, J. R., Title, A., Akin, D. J., et al. 2012, SoPh, 275, 17
Liu, Y., & Kurokawa, H. 2004, ApJ, 610, 1136
Merenda, L., Lagg, A., & Solanki, S. K. 2011, A&A, 532, 63
Nishizuka, N., Shimizu, M., Nakamura, T., et al. 2008, ApJL, 683, L83
Rust, D. M. 1968, in IAU Symp. 35, Structure and Development of Solar Active Regions, ed. K. O. Kiepenheuer (Dordrecht: Reidel), 77
Rust, D. M., Webb, D. F., & Mac Combie, W. 1977, SoPh, 54, 53
Schmahl, E. J. 1981, SoPh, 69, 135
Schou, J., Scherrer, P. H., Bush, R. I., et al. 2012, SoPh, 275, 229
Shibata, K., Ishido, Y., Acton, L. A., et al. 1992, PASJ, 44, L173
Shibata, K., Nakamura, T., Matsumoto, T., et al. 2007, Sci, 318, 1591
Shimojo, M., Shibata, K., & Harvey, K. L. 1998, SoPh, 178, 379
Sterling, A. C. 2000, SoPh, 196, 79
Vrsnak, B., Warmuth, A., Brajsa, R., & Hanslmeier, A. 2002, A&A, 394, 299
Wöger, F., & von der Lühe, O. 2007, ApOpt, 46, 8015
Zhang, J., Yang, S. H., & Jin, C. L. 2009, RAA, 9, 921